

MAGNETIC FIELDS AND LOW-FREQUENCY ACOUSTIC WAVE-ENERGY SUPPLY TO THE SOLAR CHROMOSPHERE

S.P. RAJAGURU

Indian Institute of Astrophysics, Bangalore-34, India

C.R. SANGEETHA

Inter-University Centre for Astronomy and Astrophysics, Post Bag-4, Ganeshkhind, Pune 411007, India

DURGESH TRIPATHI

Inter-University Centre for Astronomy and Astrophysics, Post Bag-4, Ganeshkhind, Pune 411007, India

Accepted for publication in The Astrophysical Journal.

ABSTRACT

The problem of solar chromospheric heating remains a challenging one with wider implications for stellar physics. Several studies in the recent past have shown that small-scale inclined magnetic field elements channel copious amount of energetic low-frequency acoustic waves, that are normally trapped below the photosphere. These magneto-acoustic waves are expected to shock at chromospheric heights contributing to chromospheric heating. In this work, exploiting simultaneous photospheric vector magnetic field, Doppler, continuum and line-core intensity (of FeI 6173 Å) observations from the Helioseismic and Magnetic Imager (HMI) and lower-atmospheric UV emission maps in the 1700 Å and 1600 Å channels of the Atmospheric Imaging Assembly (AIA), both onboard the Solar Dynamics Observatory (SDO) of NASA, we revisit the relationships between magnetic field properties (inclination and strength) and the acoustic wave propagation (phase travel time). We find that the flux of acoustic energy, in the 2 - 5 mHz frequency range, between the upper photosphere and lower chromosphere is in the range of 2.25 - 2.6 kW m⁻², which is about twice the previous estimates. We identify that the relatively less-inclined magnetic field elements in the quiet-Sun channel a significant amount of waves of frequency lower than the theoretical minimum for acoustic cut-off frequency due to magnetic inclination. We also derive indications that these waves steepen and start to dissipate within the heights ranges probed, while those let out due to inclined magnetic fields pass through. We explore connections with existing theoretical and numerical results that could explain the origin of these waves.

Keywords: Sun: chromosphere; Sun: oscillations; Sun: magnetic fields; Sun: photosphere

1. INTRODUCTION

Identifying and understanding the mechanisms of non-thermal supply of energy to the atmospheric layers (chromosphere and corona) of stars with outer convection zones so as to fully account for the observed radiative losses continue to remain a major problem in astrophysics (Narain & Ulmschneider 1996; Klimchuk 2006; Linsky 2017). There have been enormous amount of work and progress in this field, and the proposed mechanisms can be grouped under two major theories: (i) mechanical heating by waves, both non-magnetic (Biermann 1946; Schwarzschild 1948; Ulmschneider 1990) and magnetic (Alfvén 1947; Narain & Ulmschneider 1996; Ulmschneider & Musielak 2003), that are generated by turbulent convection in the photosphere and below (Lighthill 1952; Stein 1967, 1968) or by a host of magneto-hydrodynamic wave processes that couple the convection and acoustic waves to magnetic fields (Osterbrock 1961; Cally & Bogdan 1997; Rosenthal et al. 2002; Bogdan et al. 2003; Khomenko & Calvo Santamaria 2013), and (ii) direct

dissipation of magnetic energy through Joule heating, *i.e.*, resistive dissipation of electric currents, in sheared magnetic configurations and during magnetic reconnections (flares, micro- and nano-flares) (e.g., Parker 1991) with associated high speed flows and jets (see e.g., De Pontieu et al. 2004; Kashyap et al. 2013; Chandra et al. 2015; Tripathi et al. 2013, and references therein). Although the chromosphere acts as gateway to overlying hotter layers, where the above second group of processes are observed dominantly, much of the progress in the field has favoured the wave-heating mechanisms (under the first of above two theories) as the dominant ones in it (Socas-Navarro 2005; Jefferies et al. 2006; Kalkofen 2007; Straus et al. 2008). This also has some bearing on the much larger observational characterisation of stellar chromospheres through the emission in the cores of H and K lines of Ca II (Noyes et al. 1984; Kalkofen 2007): acoustic heating is thought to provide the so called 'basal flux' of emission in the above chromospheric lines in Sun-like low emission slow rotators (Schrijver et al. 1989). However, the exact nature of waves that heat the chromosphere has been brought into debate after Fossum & Carlsson (2005b) estimated that the flux of acoustic waves that reach the quiet-chromosphere (apparently non-magnetic

and hence acoustic waves of frequency larger than the quiet-Sun cut-off of 5.2 mHz) is too small to balance the radiative losses.

While the exact amount of energy flux in high-frequency acoustic waves and the dependence of its estimate on spatial resolution are still being debated (Kalkofen 2007; Bello González *et al.* 2009, 2010), the Fossum & Carlsson (2005b) result also brought into question the ‘non-magnetic chromosphere’ with the possibility that waves modified by the magnetic field might supply the required flux of energy. In this connection, the findings of Jefferies *et al.* (2006) that the small-scale inclined magnetic field elements comprising the quiet-network act as magneto-acoustic portals through which copious amount of low-frequency (2 - 5 mHz) acoustic waves propagate outward extracting energy from the acoustic reservoir below acquire prominence. Normally, acoustic waves of frequency less than the photospheric cut-off of 5.2 mHz, estimated from $\omega_{ac} = c/2H_\rho$, where c and H_ρ are the photospheric sound speed and density scale-height, respectively, are trapped below the photosphere and resonate as p modes. In the presence of magnetic fields, simple theoretical considerations (Bel & Leroy 1977) show that, when the plasma β is low ($\beta < 1$), the ω_{ac} is reduced by a factor of $\cos(\theta)$, where θ is the inclination of magnetic field with respect to the direction of gravity (local normal to the solar surface). Such effects of magnetic field have now been well attested as being responsible in a varied set of phenomena (De Pontieu *et al.* 2004, 2005; McIntosh & Jefferies 2006; Rajaguru *et al.* 2007, 2010); see also Cally *et al.* (2016, and references therein).

The previous study of energy flux in low-frequency waves in the small-scale quiet-network (Jefferies *et al.* 2006), propagating out due to reduction in acoustic cut-off frequency, used magnetic inclination angle derived from potential field extrapolation of line-of-sight (LOS) magnetic field observed by SoHO/MDI (MDI; Scherrer *et al.* 1995) with the wave-data derived from Doppler velocities observed by the South Pole instrument Magneto-Optical filter at Two Heights experiment (MOTH) (Finsterle *et al.* 2004). Similarly, the study of magnetic reduction of acoustic cut-off over a sunspot region (McIntosh & Jefferies 2006) using 1600 Å intensities from the Transition Region and Coronal Explorer (TRACE) (Handy *et al.* 1999) too utilised magnetic inclination derived from the LOS B from SoHO/MDI. In this work, exploiting simultaneous photospheric vector magnetic field, Doppler, continuum and line-core intensity (of Fe I 6173 Å) observations from the Helioseismic and Magnetic Imager (HMI) and the two lower-atmospheric UV emission maps in the 1700 Å and 1600 Å wavelength channels of the Atmospheric Imaging Assembly (AIA), both onboard the Solar Dynamics Observatory (SDO) of NASA, we revisit the relationships between magnetic field properties (inclination and strength) and the acoustic wave propagation (phase travel time). The above two instruments on the same platform provide simultaneous multi-height observations to observe the waves (through velocities and intensities) as well as the vector magnetic fields, and with higher spatial resolution than the above referred previous such studies.

In addition to our primary aim of studying (magneto-

acoustic energy supply to chromosphere via the small-scale magnetic network, in order to check and compare such processes in a range of background magnetic fluxes or sizes of structures, we include plage and spot regions too (see, e.g. review by Khomenko & Calvo Santamaria (2013)). In particular, including quiet and active Sun observations from the above described space-platform, we are able to examine closely the relationship between magnetic inclination, acoustic cut-off and height in the atmosphere, and derive acoustic wave energy flux as a function of magnetic field inclination and strength to connect with recent theoretical studies (Schunker & Cally 2006; Cally & Moradi 2013). Rest of the paper is structured as follows: in §2 we describe the data and analysis methods used in this study. In §3 we present and discuss the results in several sub-sections followed by a summary and conclusion in §3.

2. DATA AND ANALYSIS METHOD

2.1. Data

The HMI instrument uses the magnetically sensitive line Fe I 6173.34 Å for Doppler and vector magnetic field observations (Scherrer *et al.* 2012). The observables derived are photospheric continuum intensity I_c near this line, line depth L_d , Doppler velocity v_d , and magnetic field, both line-of sight B_{los} and vector. The cadence of I_c , L_d , v_d and B_{los} is 45 s. Vector magnetic field has a slower cadence of 720 s as standard pipe-line product, but can be obtained at a cadence of 135 s too (Hoeksema *et al.* 2014). The AIA observes the Sun using nine wavelength channels, namely 1700, 1600, 304, 171, 193, 211, 335, 94, & 131 Å covering different layers of the solar atmosphere (Lemen *et al.* 2012). For our purpose here, AIA observations taken in 1700 Å and 1600 Å channels that map the lower solar atmosphere are sufficient. These images are captured with a cadence of 24 s. HMI and AIA instruments observe the Sun’s disk with a pixel size of $\sim 0.5''$ and $0.6''$, respectively. Hereafter, we shall refer to the observed intensities at 1700 Å as I_{uv1} and that at 1600 Å as I_{uv2} . Since I_c is dominated by granulation (see discussion in §2.2), we add line core intensity determined as $I_{co} = I_c - L_d$ to the HMI observables used in our studies.

For the study here, we require all the above HMI and AIA observables, used to trace the waves, co-aligned and tracked with same spatial resolution. The JSOC (<http://jsoc.stanford.edu>) helioseismology pipeline facilitate this and we use it. Here, after tracking, the AIA data I_{uv1} and I_{uv2} are resampled to match the HMI cadence of 45 sec. In an earlier study of high-frequency acoustic halos (Rajaguru *et al.* 2013) such data were prepared for four large regions each covering a sunspot and quiet-Sun areas. Here, we choose two regions among them with a larger fraction of quiet-Sun network with central meridian crossing dates of 03 August 2010 and 03 July 2011. Fig. 1 displays context images of the whole Sun in LOS magnetic field corresponding to mid-time of observation period used, and the two regions studied are marked with white dashed boundaries. Note that we have displayed the magnetograms with the gray-scale saturated beyond ± 100 G so as to make the small-scale magnetic network clearly visible. The coloured boundaries (dotted lines) mark the quiet-network (blue), plage (red) and spot

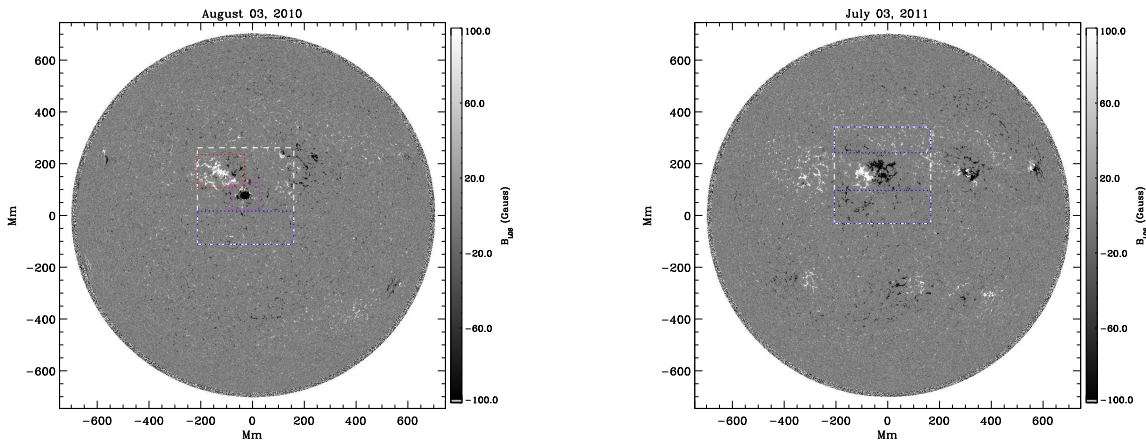


Figure 1. Context images showing the full-disk line-of-sight magnetic field, B_{LOS} , corresponding to the mid-time of observation period used in this work. The two images correspond to the two central meridian crossing dates as marked on the top of panels. Two large square regions on each date, marked by white long-dashed boundaries, are tracked in all observables used in this work. The coloured dotted-line boundaries mark the sub-regions studied in this work: regions enclosed by blue, red and pink dotted lines are the quiet, plage and spot regions, respectively. The grey-scale of the image has been saturated at ± 100 G to make the small-scale magnetic fields clearly visible.

(pink) sub-regions. Both the acoustic waves, which are excited by turbulent convection, and the quiet-Sun magnetic elements are highly dynamic and exhibit stochastic behaviour. Hence, the interaction between them, here especially the magnetic inclination caused propagation of acoustic waves that we want to track, is intermittent and stochastic (Jefferies et al. 2006); a suitable compromise for the total length of data over which the signatures of such interactions, here wave travel-times between heights and power spectrum of waves, can be averaged with sufficient signal-to-noise ratio is to be chosen. Here, for the data that we use, 14 hours is found sufficient.

The vector magnetic field over the region of study is extracted using the HMI vector-field pipeline (Hoeksema et al. 2014). It employs a Milne-Eddington based algorithm (the *Very Fast Inversion of the Stokes Vector* - VFISV: Borrero et al. (2011)) for inverting the Stokes parameters and an improved version of the *minimum energy algorithm* (Metcalf 1994; Metcalf et al. 2006; Leka et al. 2009) for resolving the 180° azimuthal ambiguity in transverse field. We use the standard 12-minute cadence vector field maps, which, over the target region, are then tracked and remapped the same way as the other data used in this study. The resulting products are the disambiguated vector field maps $[B_x, B_y, B_z]$.

For the purpose of this study (similar to Schunker & Braun (2011); Rajaguru et al. (2013)) we use a field inclination, ξ ¹ defined as $\tan(\xi) = B_z/B_h$, where $B_h = \sqrt{B_x^2 + B_y^2}$. Hence, ξ varies between $\pm 90^\circ$ with $\xi = 0^\circ$ when the field is horizontal, $\xi < 0^\circ$ when $B_z < 0$ and $\xi > 0^\circ$ when $B_z > 0$. The total magnetic field strength is $B_{tot} = \sqrt{B_x^2 + B_y^2 + B_z^2}$.

In the presence of inclined magnetic field, as briefly discussed in 1, the acoustic cut-off frequency, ν_{ac} , reduces depending on the local plasma β and the inclination, θ , of the magnetic field to the solar surface normal (direction

of gravity) (Bel & Leroy 1977); the theoretical lower limit is given by $\nu_{ac}^B = \nu_{ac} \cos\theta$. The two angles θ and ξ , then, are related as $\theta = 90^\circ - |\xi|$.

The different observables from HMI and AIA discussed above correspond to different heights in the photosphere and above. The formation process of HMI line Fe I 6173.34 Å has been studied by several authors (Norton et al. 2006; Bello González et al. 2009; Fleck et al. 2011), who derive a height range of $z = 20 - 300$ km above the continuum optical depth $\tau_c = 1$ ($z=0$ km) level with slight differences in the mean height (250 to 300 km) for the line-core formation. As to the derived observables from HMI [see Couvidat et al. (2012)], analyses comparing them with line synthesis of 3D simulations (Fleck et al. 2011; Nagashima et al. 2014) show that v_d forms at a mean height of 150 km, while the HMI line core near about 230 km; the M-E inversion algorithm is most sensitive to Stokes signals near the line-core and hence a height of 200 km is appropriate for the HMI vector magnetic field. In a detailed analysis of the performance of observables processing algorithms for HMI, Couvidat et al. (2012) found that while the derived I_c agrees well with continuum intensity near the line, line depth L_d is underestimated by about 30 - 33 %. This would then mean that, with a height of 250 km for the actual line-core, the derived line-core intensity I_{co} corresponds to a height between 0.67 to 0.7×250 which is ≈ 170 km (assuming a linear relation between height of formation and the spectral intensity within the line). The AIA 1700 Å and 1600 Å intensities [I_{uv1} and I_{uv2}], form at mean heights of 360 km and 430 km (Fossum & Carlsson 2005a), respectively.

2.2. Phase (travel-times) and Coherence Spectra

We use cross-spectra between a pair of same physical variables corresponding to two heights to derive phase travel times, t_{ph} , of waves between heights as a function of frequency, ν . Since we have velocities (v_d) at only one height, we use intensity - intensity ($I - I$)

¹ we use ξ instead of γ because the latter is commonly used for field inclination with respect to the line-of-sight

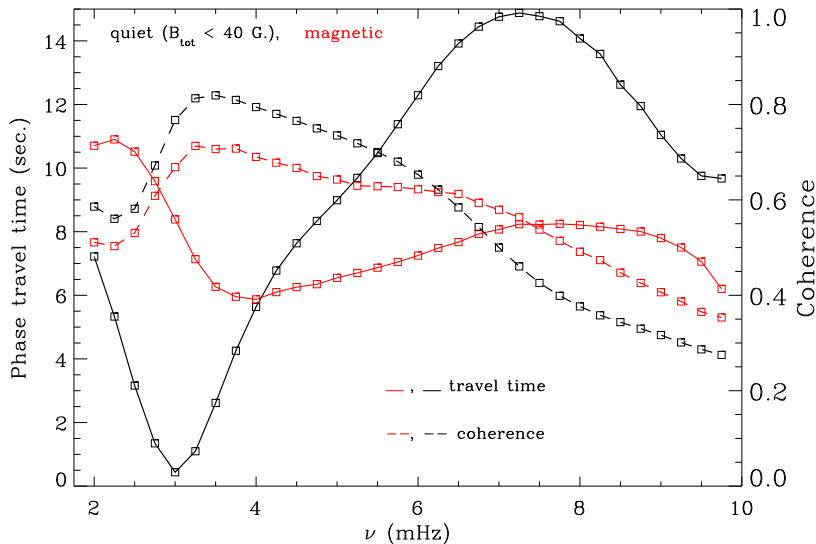


Figure 2. Quiet and magnetic area averages of t_{ph} and C against frequency ν from within the quiet-network regions enclosed by the blue dotted-line boundaries of Fig. 1.

cross-spectra. Although velocities provide less noisy capture of wave-motions, both due to p modes (helioseismic waves) that are evanescent in the photospheric layers (Duvall et al. 1993; Severino et al. 2001) and waves propagating out in the atmosphere (Jefferies et al. 2006; Bello González et al. 2009), intensities have been extensively used in studies of compressive waves in the solar atmosphere (e.g., Krijger et al. 2001; de Wijn et al. 2005; Kitagawa et al. 2010) including those that derive phase shifts over height (e.g., McIntosh & Jefferies 2006; Zhao et al. 2016). Non-adiabatic evolution due to radiative damping (RD, hereafter), however, will significantly modify the waves at heights where radiative relaxation time (Spiegel 1957), τ_R , is comparable to or shorter than wave periods, $\tau_S = 1/\nu$ (Souffrin 1972; Schmieder 1978; Webb & Roberts 1980; Deubner et al. 1990; Newington & Cally 2011). Near the transition $\tau_R \approx \tau_S$ RD can potentially be different in velocities and intensities and hence may contribute to the $I - V$ cross-spectra² (Deubner et al. 1990; Hill et al. 1991; Severino et al. 2013); in general, when $\tau_R > \tau_S$ or comparable, the acoustic cut-off frequency is not altered much and hence the character of waves, evanescent or propagating, is retained. When

² The usually observed signals in $I - V$ cross-spectra pertain to a given height or spectral line: the evanescent p modes (the 2 - 5 mHz range ridges in the $k_h - \nu$ diagram) exhibit larger than the expected adiabatic phase shifts of 90° , while the inter-ridge background region with ν less than about 3.0 mHz shows negative or near-zero phase-shifts (Deubner et al. 1990; Severino et al. 2001, 2013). Although a complete physical model capturing all the features in $I - V$ spectra is still lacking, existing literature includes successful models based on the correlated noise background (turbulent convection that excites the oscillations) to explain the inter-ridge background and modal asymmetries in the I and V power spectra (Nigam & Kosovichev 1999; Skartlien & Rast 2000) while other models that include non-adiabaticity due to radiative damping claim better match with observations (Severino et al. 2013).

$\tau_R \ll \tau_S$, apart from radiatively damping the already propagating waves (Souffrin 1972; Newington & Cally 2011) RD can also cause the evanescent waves to propagate by significantly lowering the acoustic cut-off frequency (Giovanelli et al. 1978; Roberts 1983, 2006; Centeno et al. 2006; Khomenko et al. 2008) – we discuss this further in §3.2.1 and §4 in relation to the results obtained in this work.

In the study here, however, RD *per se* does not contaminate phase shifts between heights but its height-variation, due to that in τ_R , can. Height variation of τ_R closely follows that of temperature and exhibits strong gradients close to the $\tau = 1$ photospheric region and higher up in the transition layer and corona (Schmieder 1978; Mihalas & Toomre 1982; Severino et al. 2013). In the intervening upper photospheric - lower chromospheric region, τ_R is nearly constant: between $\approx 170 - 200$ km (HMI line core intensity I_{co}) and $\approx 360 - 430$ km (AIA 1700 Å and 1600 Å) that the results in this work correspond to, we note from the realistic estimates given in Figure 4 (upper panel) of Severino et al. (2013) that τ_R is nearly constant in the range of 30 - 50 secs as compared to the wave periods of interest (180 - 500 secs). This is reflected in the nearly constant $I - V$ phase difference, between 200 - 500 km, shown in Figure 4 (lower panel) of Severino et al. (2013) for a 3.3 mHz p mode and also confirms to the results of Staiger (1985) (see also Staiger et al. (1984) and a discussion by Hill et al. (1991)) shown in Figure 1 of Deubner et al. (1990). Hence artificial phase signals due to height-dependent RD in the $I(z_1) - I(z_2)$ or $v(z_1) - v(z_2)$ phase differences between heights z_1 and z_2 in the above range should be negligible. Note that the $I - V$ phase difference itself is not the expected 90° for adiabatic evanescent p mode but it is near about $\approx 130^\circ$ which can be due to RD (Severino et al. 2013), but the relevant fact here is that this value remains roughly constant over the height range

considered here. This assessment is further substantiated in §3.1, where we show that quiet-Sun phase shifts derived from intensities match very closely those from velocities over a similar height range (Wiśniewska et al. 2016).

The two-height cross-spectra here are between two time-series, and are calculated at each location (pixel). Hence the derived t_{ph} are maps, i.e., $t_{\text{ph}}(x, y, \nu)$ where x and y are the spatial coordinates. The cross-spectrum of two time-series I_1 and I_2 is defined as the complex-valued product of the Fourier transforms of the two series,

$$X_{12}(\nu) = \mathbf{I}_1(\nu)\mathbf{I}_2^*(\nu) \quad (1)$$

where \mathbf{I} 's are the Fourier transforms; * represents the complex conjugate. The phase-lag, $\delta\phi$, between the two time-series is then given by the phase of the complex cross-spectrum $X_{12}(\nu)$,

$$\delta\phi(\nu) = \tan^{-1}[\text{Im}(\langle X_{12}(\nu) \rangle)/\text{Re}(\langle X_{12}(\nu) \rangle)] \quad (2)$$

The magnitude of $X_{12}(\nu)$ is used to calculate the coherence,

$$C(\nu) = \frac{|\langle X_{12}(\nu) \rangle|^2}{\langle |\mathbf{I}_1|^2 \rangle \langle |\mathbf{I}_2|^2 \rangle}, \quad (3)$$

which ranges from 0 to 1 and is a measure of linear correlation between I_1 and I_2 . In the above two equations, $\langle . \rangle$ denotes ensemble average or expectation value, which requires averaging over realisations. In our case here, each realisation corresponds to a wave-process in which an acoustic wave, recorded in I_1 , hits the magnetic field, which depending on its inclination to solar normal (and to the wave-vector) lets it propagate outward to a height where it is recorded as I_2 . For a single realisation of a wave connecting the two heights, coherence at a frequency is unity. Normally, a frequency averaging is performed to estimate coherence. Given a granular lifetime of 10 minutes, and that we are mainly interested in acoustic waves of periods in the range of 3 - 10 minutes (1.5 - 5.2 mHz), we do have a large number of independent realisations of the above wave-process in the 14-hour long observations that we use. Hence, to achieve the above ensemble averaging, we split the time-series into segments of equal length of about 96 mins (corresponding to 128 data points in the 45 sec. cadence data) and calculate cross-spectra for each segment and then average them together. We believe that this way of estimating $\delta\phi$ and C does better justice to the dynamic and intermittent nature of interactions between the magnetic field and acoustic waves. The basic cross-spectral estimation as above is implemented using a IDL (Interactive Data Language) code by Simon Vaughan available at <https://github.com/svdataman/IDL>.

The phase travel times, t_{ph} , as a function of frequency ν are simply the time lags corresponding to $\delta\phi$ determined as,

$$t_{\text{ph}}(\nu) = \frac{\delta\phi(\nu)}{2\pi\nu} \quad (4)$$

In our convention in Eq.(1), a positive t_{ph} (or $\delta\phi$) means that I_1 leads I_2 in phase and hence corresponds to waves propagating upward and vice versa. The photospheric continuum intensity I_c is dominated by granulation, and since granules have lifetimes of the order of 5 to 10 minutes, the same as wave periods, they swamp the phase signals due to waves if we use it in $I - I$ cross-spectra.

Hence, we restrict to using the intensity pairs $I_{\text{co}} - I_{\text{uv}1}$ and $I_{\text{co}} - I_{\text{uv}2}$ to calculate cross-spectra and estimate t_{ph} ; these, then, correspond to following waves from upper photosphere to chromospheric layers in the height range of 170 - 360 km and 170 - 430 km, respectively. Between the photosphere and chromosphere, the $\delta\phi$ or t_{ph} receive a dominant negative contribution from atmospheric gravity waves, which occupy the region of smaller frequencies bounded by the f -mode (surface-gravity mode) ridge in the $k_{\text{h}} - \nu$ dispersion diagram (see, e.g. Straus et al. 2008, and references therein). These gravity waves have downward phase propagation (hence negative t_{ph}) while transporting energy upward. Since we are interested in acoustic wave propagation, we first apply a helioseismic filter [a 3D Fourier filter in (ν, k_x, k_y)] to the basic data cubes to remove the surface- and atmospheric-gravity waves (Giles 2000; Rajaguru et al. 2004) before using them in the above cross-spectral analysis.

2.3. Estimating Energy Fluxes

Energy fluxes at heights 360 and 430 km corresponding to $I_{\text{uv}1}$ and $I_{\text{uv}2}$ are calculated using the estimates of t_{ph} from the cross-spectra of intensity pairs $I_{\text{co}} - I_{\text{uv}1}$ and $I_{\text{co}} - I_{\text{uv}2}$ as follows (following the same basic principles as in Jefferies et al. (2006)). The basic expression that we use to determine energy flux F at height z is (Canfield & Musman 1973; De Moortel & Rosner 2007; Jefferies et al. 2006),

$$F(z) = P(z) v_{\text{g}}(z) \rho(z), \quad (5)$$

where P is wave-velocity power, ρ is the plasma density and v_{g} is the group velocity of the waves. We use density values from the FAL 93 models (Fontenla et al. 1993) the same way as Jefferies et al. (2006). Group velocities at a given height are estimated from t_{ph} at that height using,

$$v_{\text{g}}(z) = \frac{c^2 t_{\text{ph}}(z)}{\Delta z}, \quad (6)$$

where c is the sound speed, Δz is the height difference that t_{ph} corresponds to. For t_{ph} from the cross-spectral pairs $I_{\text{co}} - I_{\text{uv}1}$ and $I_{\text{co}} - I_{\text{uv}2}$, the Δz 's are 190 km and 260 km, respectively. We use $c = 7$ km/sec, which is appropriate for lower solar atmosphere. Note that the power P in Eq.(5) has to be estimated at the height of t_{ph} , but we have only the photospheric velocities v_{d} and hence $P_{\text{HMI}} = \langle v_{\text{d}}^2 \rangle$. However, spatial map of t_{ph} allows us to estimate $P(z)$ using the height evolution of velocities for propagating and evanescent waves (see, e.g. Christensen-Dalsgaard 2003): conservation of mechanical energy flux dictates that the velocity amplitudes of propagating waves change as $v(z) = v_{\text{d}} \exp[\Delta z_{\nu}/2H_{\rho}]$ while those of evanescent waves ($\nu < \nu_{\text{ac}}$) decay as $v(z) = v_{\text{d}} \exp[-\Delta z_{\nu}(1 - \nu^2/\nu_{\text{ac}}^2)^{1/2}/2H_{\rho}]$, where $\Delta z_{\nu} = z - z_{\text{d}}$ is the height referenced to that of v_{d} . Here, with $z_{\text{d}} = 150$ km for HMI velocity and $z = 360$ km or 430 km for $I_{\text{uv}1}$ or $I_{\text{uv}2}$, we have $\Delta z_{\nu} = 210$ km or 280 km, respectively. To apply the former increasing amplitude against height, locations of upward propagation are identified as those having $t_{\text{ph}} \geq \sigma_{\text{q}}^t$, the standard deviation of t_{ph} over all quiet (non-magnetic) locations with HMI (time-averaged) B_{tot} less than 40 G. Since the propagation in height is mainly within magnetic fields, we need to consider the modification in height evolution caused by magnetic fields:

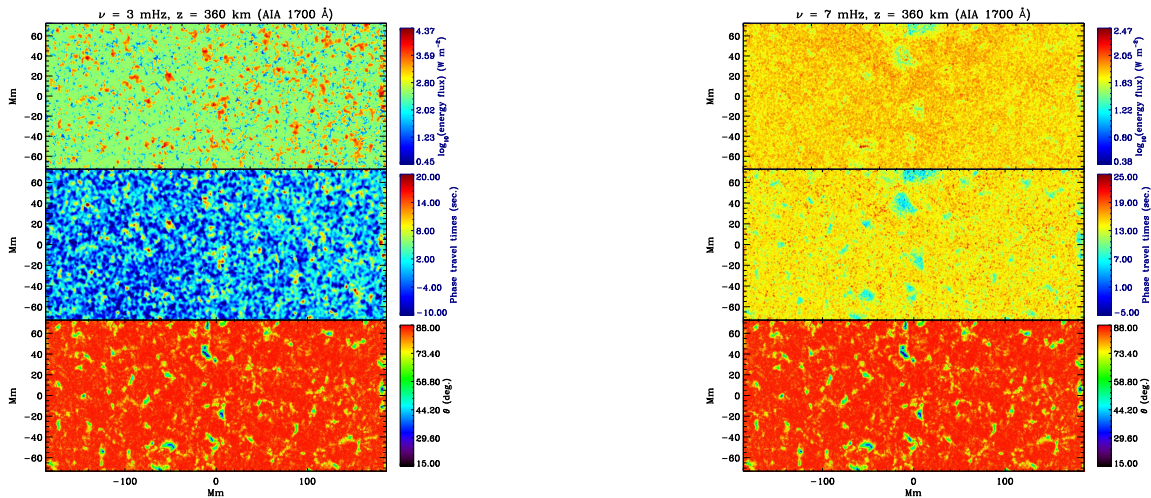


Figure 3. Maps of magnetic inclination angle θ (bottom panel), phase travel time t_{ph} (middle panel), and logarithm of energy flux F over the quiet-network area of August 3, 2010 region shown in Fig. 1. The t_{ph} and F are for acoustic waves of frequency 3 mHz (left set of panels) and 7 mHz (right set of panels) propagating from 170 km (HMI line-core intensity I_{CO}) to 360 km (AIA 1700 Å intensity I_{UV1}).

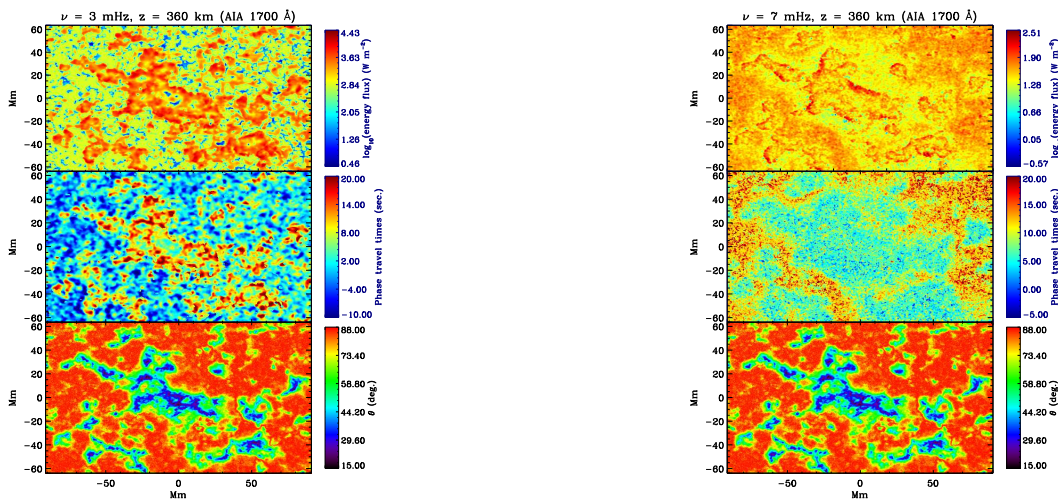


Figure 4. The same as Fig. 3 but for the plage region of August 3, 2010 shown in Fig. 1.

solutions for longitudinal waves within vertically oriented flux tubes give a height dependence $\exp[\Delta z_{\nu}/4H_{\rho}]$ (Spruit 1981), which arises from the height variation of magnetic field. For power, just the squares of the above exponential height-evolution factors multiply P_{HMI} to give $P(z)$. In addition, since we are largely tracking acoustic waves travelling along the magnetic field, we correct for the underestimation of v_{d} (which is *LOS* velocity) by $\cos(\theta)$ factor due to magnetic field inclination θ . Estimates of t_{ph} , and $P(z)$ from P_{HMI} as described above, at two heights 360 and 430 km corresponding to I_{UV1} and I_{UV2} are done in Fourier space at each frequency, and hence the above procedure gives maps of energy fluxes, $F(x, y, \nu)$, at these two heights.

Energy fluxes estimated by the above method, clearly, have a uncertainty range determined by that in Δz , Δz_{ν} and that for H_{ρ} . While Δz enters through v_{g} , the other ones, through the exponential factors discussed above, determine $P(z)$. Moreover, spatial resolution of the data too play a role in energy estimates (Jefferies et al. 2006; Kalkofen 2007; Bello González et al. 2009, 2010). Much of the differences due to spatial resolution in the esti-

mates of above authors have been for waves of frequencies larger than the quiet-Sun acoustic cut-off $\nu_{\text{ac}} = 5.2$ mHz. To assess the relative contribution of lower frequency, $\nu < \nu_{\text{ac}}$, waves transmitted out by the quiet-Sun inclined magnetic fields, Jefferies et al. (2006) calibrated their estimates by scaling them to match their higher-frequency (5.2 - 10 mHz) energy fluxes with that of Fossum & Carlsson (2005b), who had higher spatial resolution (0.6'' resolution TRACE 1700 Å and 1600 Å observations) and had validated their estimates with numerical simulations. Over 5.2 - 10 mHz, quiet-Sun mean energy flux determined by these authors was 286.9 W m^{-2} (Jefferies et al. 2006). With the same spatial resolution and for the same chromospheric height probed by 1700 Å (but here from SDO/AIA), our calculations yield very closely the same value (286.2 W m^{-2} , see Figure 11, left panel) when we use $\exp[\Delta z_{\nu}/4H_{\rho}]$, with $H_{\rho} = 110$ km, to determine wave velocities at height Δz_{ν} above z_{d} using HMI velocities v_{d} . The adopted value for H_{ρ} agrees well with the FAL 93 models (Fontenla et al. 1993), which give $H_{\rho} \approx 109$ km for the non-magnetic model (Model C) and ≈ 120 km for the magnetic model

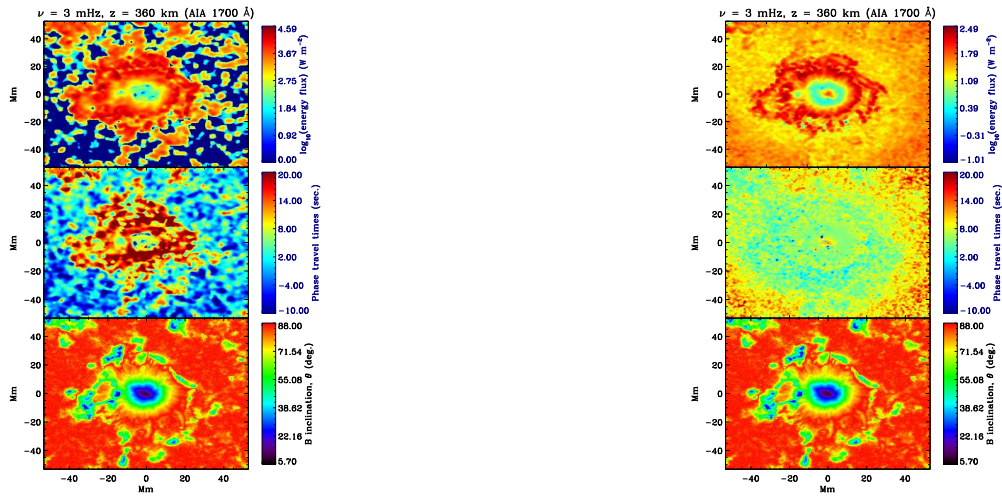


Figure 5. The same as Fig. 3 but for the spot region of August 3, 2010 shown in Fig. 1.

(Model P) for heights in the range of 150 - 450 km.

It should be noted that the magnetic modification that halves the rate at which velocities increase over height, with $4H_\rho$ scaling of height instead of $2H_\rho$ in $\exp[\Delta z_\nu/4H_\rho]$, is appropriate only for $\nu < \nu_{ac}$ as otherwise all higher ν waves propagate in the non-magnetic atmosphere. Hence, noting that power P involves squares of the above exponential factors, a more realistic value for the 5.2 - 10 mHz mean energy flux in our calculations would be $\exp[\Delta z_\nu/2H_\rho] \times 286.2 = 743.0 \text{ W m}^{-2}$, for $\Delta z_\nu = 210 \text{ km}$ (*i.e.*, $z = 360 \text{ km}$, AIA 1700 Å). On the other hand, as discussed in §2.2, we are in the regime of $\tau_R < \tau_S$, and hence RD will amount to a reduction in amplitudes over height faster than $\exp[\Delta z_\nu/2H_\rho]$, and this possibly explains the lower value of 286.9 W m^{-2} obtained by Fossum & Carlsson (2005b). We stress, however, the importance of accounting for the magnetically confined propagation of acoustic waves for $\nu < \nu_{ac}$ through the use of $\exp[\Delta z_\nu/4H_\rho]$ in calculating velocities over height Δz_ν . The resulting mean energy fluxes over 2 - 5.2 mHz range are presented and discussed in §3.3. We further note that, since extending the above to quiet-Sun propagation at $\nu > \nu_{ac}$ leads to an underestimation by nearly a factor of e , but matches with that of Fossum & Carlsson (2005b) without any additional scaling as done by Jefferies et al. (2006) to calibrate their estimates, our estimates for the lower frequencies are likely to be conservative or lower limits.

3. RESULTS AND DISCUSSIONS

3.1. Maps of Phase Travel-times and Energy Fluxes

The phase travel-times t_{ph} and coherence C , as described in §2.2, are estimated at the two heights, 360 and 430 km, over the two regions shown in Figure 1. Before analysing the variations of t_{ph} against B_{tot} and θ , we first check if the quiet-Sun changes in t_{ph} against frequency ν confirm with the expected behaviour without much contamination due to height-dependent RD, as discussed in §2.2. Within the quiet-Sun areas marked in Figure 1 with blue boundaries, we separate the magnetic and non-magnetic pixels with the criterion of $B_{tot} < 40 \text{ G}$ for the latter and then average t_{ph} and C over these two groups of pixels. The results are shown in Figure 2. The ν variation of quiet-Sun travel times (or phase difference

against height) shows the familiar trend, with the main p-mode band showing the evanescent behaviour: smaller or close-to-zero t_{ph} within the 2 - 5 mHz with the smallest values at 3 mHz, and correspondingly large coherence (peak values of 0.8 near 3 mHz). The magnitudes and ν dependence of quiet-Sun t_{ph} obtained here match very closely the recent estimates, for the same height range, from multi-height velocity data (Wiśniewska et al. 2016). Overplotted in Figure 2 are the ν variations of t_{ph} and C averaged over magnetic pixels. The magnetic field assisted propagation is clear in the enhanced low-frequency travel times – this is the turn-on of propagation due to reduction of acoustic cut-off frequency by the inclined magnetic fields (Jefferies et al. 2006); we explore in detail this behaviour in the rest of the paper, including revised estimates of energy fluxes. Note that, in Figure 2, we have not separated the phase shifts over inclined and near-vertical fields as in Jefferies et al. (2006) but do a detailed analysis of dependence on θ in §3.2 (see Figure 6), where a good agreement with Jefferies et al. (2006) is found for inclined magnetic fields while uncovering some new features in the nearly vertical small-scale fields. As argued in §2.2, the above described agreement between $I(z_1) - I(z_2)$ phase shifts derived here and the $V(z_1) - V(z_2)$ phase shifts of Wiśniewska et al. (2016) and Jefferies et al. (2006) for the quiet-Sun evanescent and the magnetic inclination-assisted propagation, respectively, in the frequency range 2 - 5 mHz shows that the height dependence of RD plays negligible roles. We stress that only the height dependence of RD and hence contamination or artificial phase shift due to it is negligible, but RD itself is significant as $\tau_R < \tau_S$ in the height ranges considered and hence the real physical effect of lowered acoustic cut-off is still possible. This we believe is why the quiet-Sun curve (Figure 2), similar to the results of Wiśniewska et al. (2016), exhibits significant propagation (non-zero t_{ph}) down to about $\approx 4 \text{ mHz}$, while the usual theoretical value for acoustic cut-off is $\nu_{ac} = 5.2 \text{ mHz}$. It is to be noted that the coherence values, on average, remain largely above 0.5 over quiet and magnetic pixels (except at high frequencies), and hence the estimates of t_{ph} can reliably be attributed to waves; for estimates of mean energy fluxes (over observed areas) we apply a correction for pixels with low coherence (see next

Section).

We show in Figures 3 - 5 the 3 and 7 mHz maps of travel-times t_{ph} and energy fluxes F , along with that of magnetic inclination θ , for the quiet-Sun, plage and spot areas of the *03 Aug 2010* region (marked in Figure 1). These maps portray striking variations and patterns as a function of frequency and background magnetic structures. At frequencies lower than ν_{ac} ($= 5.2$ mHz), it is readily recognised that t_{ph} and F are concentrated within the discrete magnetic field elements of the quiet-Sun (*left panel* of Figure 3), confirming what Jefferies *et al.* (2006) described as magneto-acoustic portals. In the plage (*left panel*, Figure 4) and sunspot (*left panel*, Figure 5) regions, however, the lower frequency enhancements are larger in the more inclined boundary regions of magnetic flux concentrations. At frequencies larger than ν_{ac} (refer to the 7 mHz maps in the *right panels* of Figures 3 - 5), all magnetic flux concentrations exhibit a nulling or much reduced t_{ph} around them, *i.e.* in the inclined canopy regions, and correspondingly there is much reduced upward energy flux. This phenomenon around small-scale magnetic fields at chromospheric heights was observed in high-resolution by Vecchio *et al.* (2007). At the photospheric and upper photospheric levels, these signatures in t_{ph} spatially coincide with the so called *acoustic halos* that represent enhanced oscillation power (see, Rajaguru *et al.* 2013, and references therein). This reduction or nulling of t_{ph} has been modeled and interpreted as due to mode-conversion assisted horizontal (Nutto *et al.* 2012) or downward propagation of fast magnetoc-acoustic waves at the canopy (Rijs *et al.* 2016). Another feature in the larger flux concentrations, especially in the sunspot, is the pattern of increasing frequencies from the outer edge (3 mHz in more inclined fields) towards the central (> 5 mHz in the nearly vertical umbral fields) region (refer to the *right panels* in Figure 5). This feature has also been observed earlier in different contexts (Zhao *et al.* 2016; Jess *et al.* 2016) – a more detailed examination of this and its relation to θ and ν_{ac}^B is presented in the next Section.

It is to be noted that, although we have filtered out the low-frequency atmospheric gravity modes (*cf.*, §2.2), the maps of t_{ph} (middle panels of Figures 3 - 5) still show significant areas of negative values (corresponding to downward propagation) at low frequencies (2 - 4 mHz). In general, $k - \nu$ cross-spectra of two-height oscillation data (in intensities as well as velocities) have been known to show negative phase-differences between evanescent (*i.e.*, zero phase-difference) p mode ridges, but their origin is not understood (see, Krijger *et al.* 2001; Severino *et al.* 2013; Nagashima *et al.* 2014, and references therein). The spatial average of t_{ph} over all quiet non-magnetic pixels, however, show the nearly evanescent behaviour in 2 - 4 mHz range (see Figure 2). In the top panels showing energy fluxes F in Figures 3 and 4, for the purpose of display, we have replaced all the negative t_{ph} locations within the non-magnetic quiet area by that F estimated using the quiet-Sun average values shown in Figure 2.

3.2. Magnetic Inclination and Strength Dependences of Wave Propagation

Effects of magnetic fields on wave-propagation and energy fluxes are studied by deriving the variation of t_{ph} and F against θ and B_{tot} at each ν . For this purpose,

we group (and average) pixels in the 2D maps $t_{\text{ph}}(x, y)$ and $F(x, y)$ (Figures 3 - 5) over bins of 4° in θ and 30 G in B_{tot} . Although, on average, coherence $C > 0.4$ over much of the frequency ranges considered here, there are significant quiet- as well as magnetic locations with lower C , and hence we select only those locations where $C > 0.4$ for deriving the dependences on θ and B_{tot} . The results are 2D functions $t_{\text{ph}}(\theta, \nu)$, $t_{\text{ph}}(B_{\text{tot}}, \nu)$, $F(\theta, \nu)$, and $F(B_{\text{tot}}, \nu)$ shown in Figures 6 - 8: quiet and plage regions' results are plotted in the same set of panels in Figures 6 and 7, the spot region is plotted separately in Figure 8. The two sets of panels in Figures 6 and 7 show t_{ph} and F at heights 360 km (1700 Å) and 430 km (1600 Å); in each set the upper sub-panels show $t_{\text{ph}}(\theta, \nu)$ or $t_{\text{ph}}(B_{\text{tot}}, \nu)$, and the lower ones $F(\theta, \nu)$ or $F(B_{\text{tot}}, \nu)$ for the quiet and plage regions.

3.2.1. Phase Travel-times

The inclination θ of magnetic fields to the direction of gravity, as referred to earlier in §2.1, reduces the effective gravity that the fluid tied to the magnetic field is subject to by a factor $\approx \cos(\theta)$ and hence the acoustic cut-off frequency, ν_{ac} , that is proportional to the acceleration due to gravity g is similarly reduced (Bel & Leroy 1977). We have overplotted the theoretical minimum $\nu_{\text{ac}}^B = \nu_{\text{ac}} \cos \theta$ due to magnetic fields in the maps of $t_{\text{ph}}(\theta, \nu)$ in Figures 6 - 8 as dashed curves. The region of smaller θ and ν bounded by this curve in the $\theta - \nu$ plane, in principle, is not accessible for wave-propagation via reduction in ν_{ac} due to magnetic inclination θ . However, Figure 6 shows that, strikingly, almost the whole of this region of low ν and $\theta < 60^\circ$ is filled with propagating waves in the case of lower height (360 km, 1700 Å) $t_{\text{ph}}(\theta, \nu)$ corresponding to quiet-network (the top left sub-panel in Figure 6; note also the different ranges of color-scales for t_{ph} in the left and right set of panels). It is to be noted that locations where $\theta > 80^\circ$ correspond to very weak magnetic fields or completely quiet, and the $\theta - \nu$ behaviour of t_{ph} in this region (in Figures 6 and 7) is, overall, consistent with that expected in quiet-Sun: propagation at frequencies > 5 mHz, largely, and evanescent behaviour otherwise, with a caveat that, similar to the results of Wiśniewska *et al.* (2016), the quiet-Sun acoustic cut-off is lower than the usual theoretical value of $\nu_{\text{ac}} = 5.2$ mHz with non-zero propagation down to about ≈ 4 mHz at $\theta > 80^\circ$.

The above described propagation in the low ν (2 - 4 mHz) and largely in the less inclined (from nearly vertical $\theta \approx 10^\circ$ to $\theta < 60^\circ$) region over the quiet magnetic-network is distinct from that could be explained by any modification or reduction of acoustic cut-off. The corresponding signatures are also clear in $t_{\text{ph}}(B_{\text{tot}}, \nu)$ shown in the top left sub-panels of Figure 7: stronger (> 500 G), less inclined fields show enhanced t_{ph} . Further, over height, this propagation region diminishes both in $t_{\text{ph}}(\theta, \nu)$ and $t_{\text{ph}}(B_{\text{tot}}, \nu)$: at height 430 km (1600 Å) the t_{ph} in 2 - 4 mHz region, for both the quiet-network and the plage, do not show an increase expected over height, and in fact there is a slight reduction at the lowest frequencies. This is possible only if all of the propagating waves seen at the lower height do not reach the higher location, in turn implying wave steepening and dissipation (Krijger *et al.* 2001). To see the changes over height clearly, we have plotted the height difference in t_{ph} , *i.e.*, difference between the 430 km (1600 Å) and 360 km (1700 Å) t_{ph}

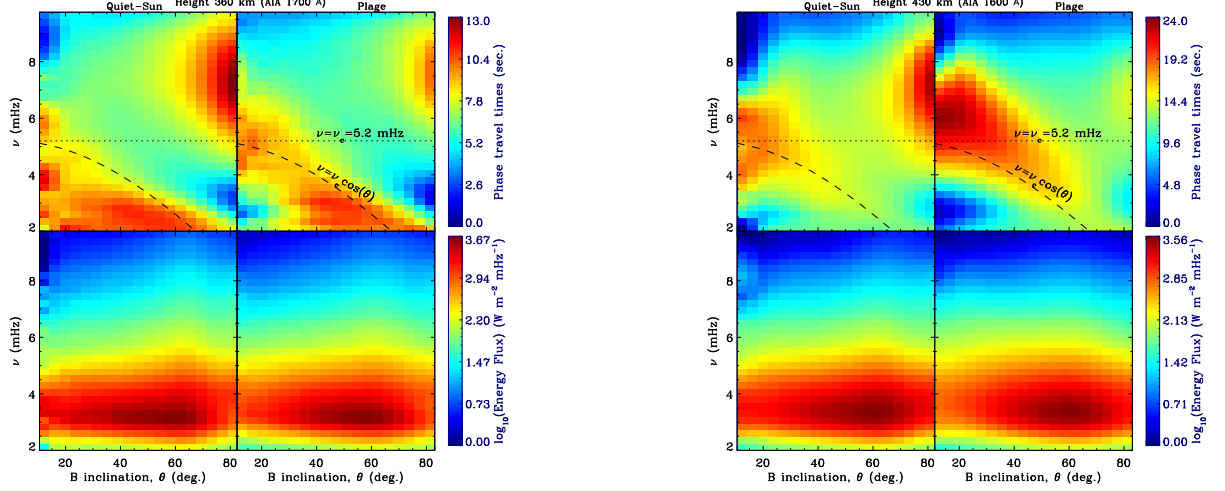


Figure 6. Phase travel times, t_{ph} , and logarithm of energy fluxes, F , against magnetic inclination angle, θ , and wave frequency, ν , compared for quiet and plage regions; left set of panels is for AIA 1700 Å height (360 km) and that on the right is for AIA 1600 Å height (430 km).

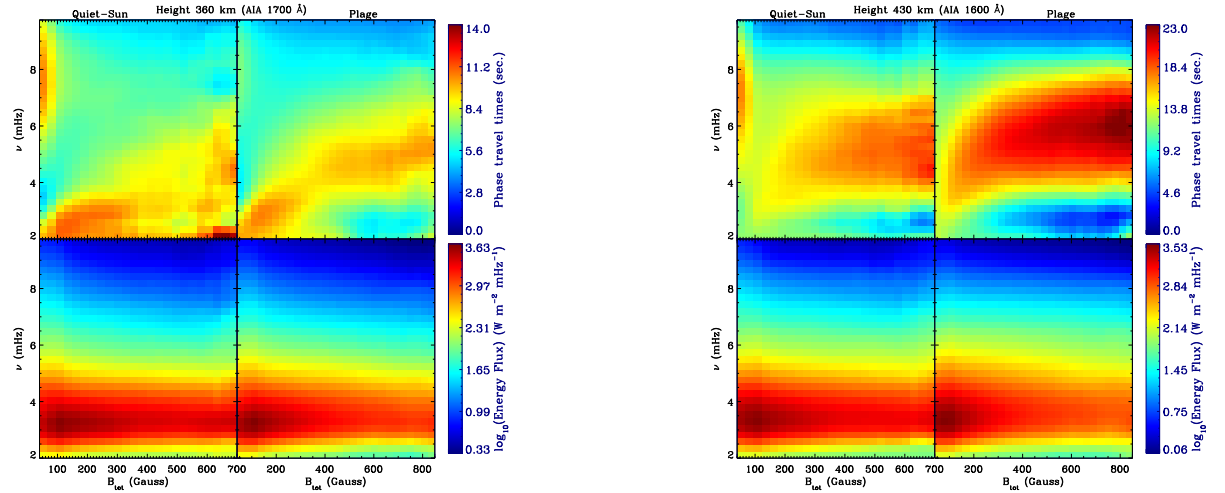


Figure 7. Phase travel times, t_{ph} , and logarithm of energy fluxes, F , against total magnetic field strength, B_{tot} , and wave frequency, ν , compared for quiet and plage regions; left set of panels is for AIA 1700 Å height (360 km) and that on the right is for AIA 1600 Å height (430 km).

shown in the top left panels of Figure 6, averaged over $\theta < \theta_{ac} = \cos^{-1}(\nu/\nu_{ac})$ and over $\theta \geq \theta_{ac}$ in the left panel of Figure 9: it is clear that waves in the (θ, ν) space allowed via reduced ν_{ac} due to magnetic inclination propagate to heights above 430 km (dashed curve), whereas that in the region of smaller θ and ν bounded by ν_{ac}^B have smaller t_{ph} (solid curve) for the same height difference indicating wave steepening. This then implies that waves propagating in the region $\theta < \theta_{ac}$ evolve faster to shock at lower chromospheric heights. A similar θ -integration of energy fluxes F (corresponding to the lower left panels of Figure 6) and ratios of them are shown in the right panel of Figure 9 and are discussed in §3.3.

Given that the small-scale magnetic flux elements are highly dynamic, one can argue that the propagation region of $\theta - \nu$ in Figure 6 (top left panel) is actually due to the intermittent excursions to large inclinations (beyond the dashed curve) of a flux element, while its average θ (used in the analyses here) remains low. To check this, we plot the standard deviation of θ over the full time-length of data used (at 720 sec. cadence) against the mean θ

in Figure 10: the light blue band shows the extent or distribution of standard deviation over the duration of observation at each location that has the mean θ (shown in the x -axis). The green dots running at the center of the blue band are the RMS of standard deviation at 2° interval. Up to about $\theta = 30^\circ$ the maximum standard deviation is less than 20° , and hence flux elements with average inclinations less than 30° still do not reach inclinations $\theta > 50^\circ$ to allow propagation at frequencies 3.3 mHz and lower. Hence, the dynamic nature of flux elements is still not sufficient enough to cause the low ν (2 - 4 mHz) and $\theta < 40^\circ$ propagation seen in Figure 6.

Although we have verified in §3.1 that RD has not contaminated (*i.e.*, introduced artifacts in) the quiet-Sun t_{ph} confirming our identification in §2.2 that τ_R is nearly constant over the height ranges considered, we still need to address if the nearly vertical network flux tubes present suitable physical conditions so different from the quiet-Sun that either (i) artifacts of height dependent RD, or (ii) a large reduction in acoustic cut-off due to strong RD (Giovannelli et al. 1978; Roberts 1983; Centeno et al.

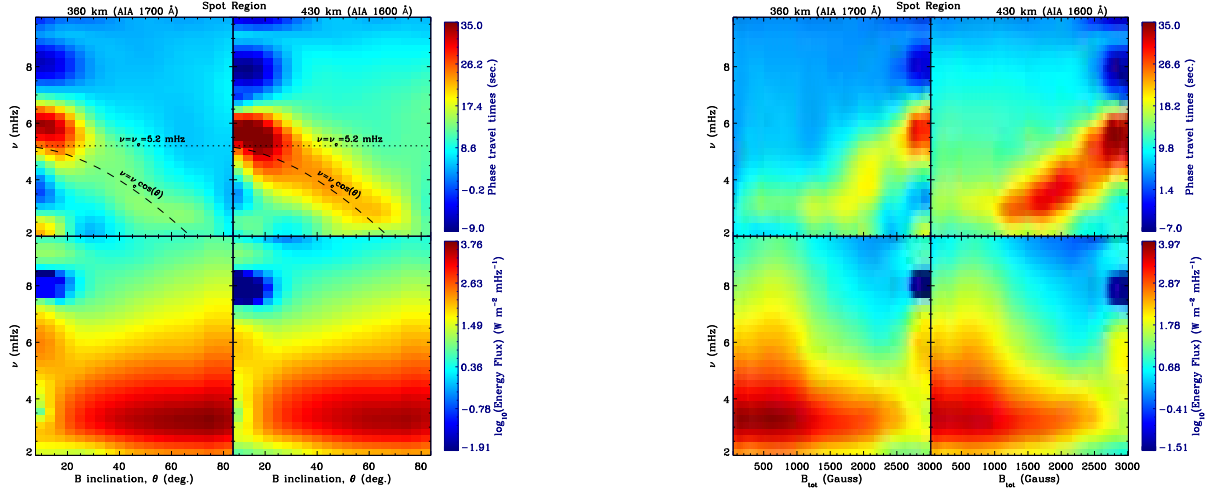


Figure 8. Phase travel times, t_{ph} , and logarithm of energy fluxes, F , against magnetic inclination angle θ and wave frequency ν (left set of panels), and against total magnetic field strength B_{tot} and wave frequency ν (right set of panels) for the spot region.

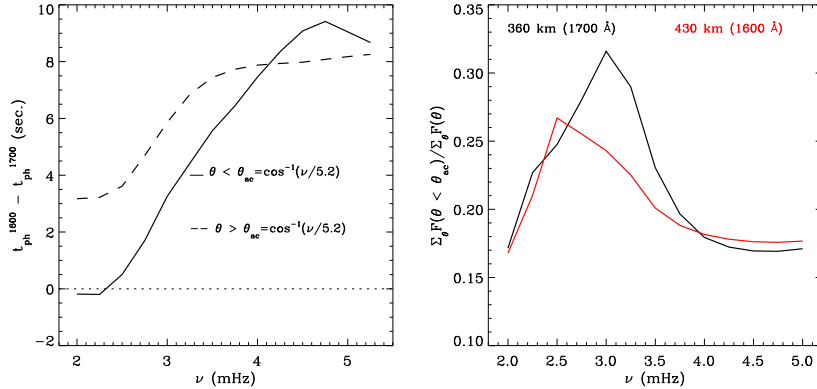


Figure 9. *Left panel:* differences in t_{ph} , averaged over $\theta < \theta_{ac} = \cos^{-1}(\nu/\nu_{ac})$ and over $\theta \geq \theta_{ac}$, of 430 km (1600 Å) and 360 km (1700 Å) heights shown in the top left panels of Figure 6. *Right panel:* ratios of energy fluxes F integrated over $\theta < \theta_{ac}$ to that integrated over the whole range. See §3.3 for details.

2006; Khomenko et al. 2008) could be responsible for the above 2 - 4 mHz propagation.

In case (i), we have the situation that the 2 - 4 mHz waves inside vertical tubes are in fact evanescent but the detection method picks up a positive phase-shift as an artifact mimicking upward propagation; this can happen only if RD increases via a decreasing τ_R over height inside the flux tube, in contrast to the opposite trend of slightly increasing τ_R in the quiet-Sun over the height ranges covered here (Mihalas & Toomre 1982; Newington & Cally 2011; Severino et al. 2013). Further, as seen in Figure 6 (top left panel), the 2 - 4 mHz phase shifts over $\theta < 40^\circ$ is nearly two to five times that in the quiet-Sun and as we discuss below the vertical fields within the plage region do not show such propagation (Figure 6, top right

panel). Hence the decrease in τ_R over height within isolated flux tubes has to be of large magnitude and vastly different from not only that in quiet-Sun but also from plage region. This highly contrived situation within only the small-scale network elements is highly unlikely.

For case (ii), although the requirement is less stringent in that it concerns only the physical effect depending on the magnitude of RD, a large reduction in τ_R within network flux tubes as compared to quiet-Sun or even the vertical fields of plages is still needed. We note that Centeno et al. (2006) and Khomenko et al. (2008) have reported observations with models based on case (ii) but over heights between 400 - 1500 km; these heights mostly lie above the region covered in this work, and further since the vertical flux tubes expand rapidly over height to

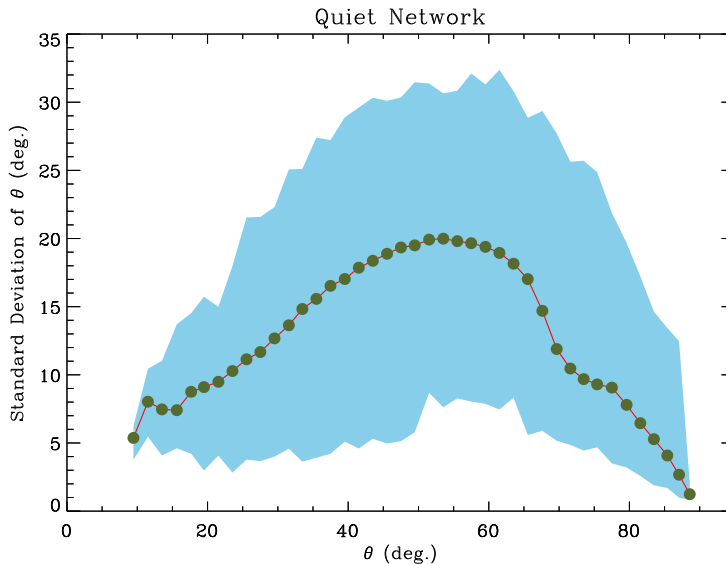


Figure 10. The standard deviation of θ against the mean θ in the quiet magnetic-network. The light blue band shows the extent of standard deviation over the duration of observation at each location that has the mean θ (shown in the x - axis).

fill the chromosphere at these heights, it becomes difficult to differentiate waves propagating due to RD with those due to magnetic inclination. Moreover, these authors report phase delays peaking around 3 mHz, which they achieve as a reduced cut-off frequency within magnetic tubes due to RD in their models with $\tau_R = 10$ sec as compared to 50 sec outside quiet-Sun. We note that our results (Figure 2 and top left panel of Figure 6) require cut-off frequency reduction to a value less than 2 mHz and hence a value for τ_R even smaller than 10 sec, which may be unrealistic. We, however, identify that the theoretical treatment of the longitudinal tube mode (or the sausage mode) subject to RD by Roberts (1983) provides a formula for cut-off frequency that yields numbers differing from that obtained for the acoustic-gravity mode within the 2D magnetic flux tubes treated by Khomenko et al. (2008), and provides a better match to the observations here: under the near-isothermal photospheric conditions, Eqn. (30) of Roberts (1983) yields for the tube cut-off frequency, $\omega_{tc} = c_T/2H_p$, where H_p is the pressure scale-height, c_T is the tube speed given by $c_T^2 = c^2 v_A^2 / (c^2 + v_A^2)$ and v_A is the Alfvén speed. The tube speed c_T in general, for photospheric conditions of $v_A \approx c$, is lower than both c and v_A . Noting that without RD the tube cut-off is almost the same as the quiet-Sun cut-off of 5.2 mHz (Spruit 1981; Roberts 1983), the above limit for tube cut-off under RD in isothermal conditions yields $\omega_{tc} \approx 1.3$ mHz, with $H_p = 150$ km, $c_T = 5$ km s $^{-1}$ and $v_A^2 = c^2 = \gamma g H_p$, γ and g being the adiabatic index and acceleration due to gravity. We also note that the early observations by Giovanelli et al. (1978) has considerable overlap with the height ranges covered in this work, and agree better with the results for t_{ph} in quiet-Sun network magnetic fields. In any case, it is clear from the whole scenario above that a mechanism different from that of magnetic inclination assisted channeling of ambient acoustic waves to generate the observed (Figure 6, top left panel) low-frequency

(2 - 4 mHz) waves within the small-scale less-inclined or nearly vertical quiet-network magnetic fields is necessary. We come back to this aspect and discuss this further in relation to the vast amount of work that addresses generation of waves within flux tubes or sheaths in §4.

In the plage and spot regions, as depicted in the top right sub-panels of Figures 6 and 7 and the top panels of Figure 8, $t_{ph}(\theta, \nu)$ and $t_{ph}(B_{tot}, \nu)$ show striking differences in their character as compared to the quiet-network. Firstly, the nearly vertical ($\theta < 30^\circ$) core regions of these large magnetic structures show much reduced or no propagation signals in the 2 - 4 mHz range indicating a similarly reduced vigour or the absence of the wave-generation process, that we inferred for the small-scale quiet-network fields. Secondly, almost all of the low-frequency propagation signals show a tight correlation with the cut-off frequency reduction according to $\nu_{ac}^B = \nu_{ac} \cos \theta$: this is especially clear in the 430 km (1600 Å) results in the top right sub-panels of Figures 6 and 7 for plages and the top panels of Figure 8 for the sunspot. These dominant influences of magnetic inclination θ cause the spatial pattern of smallest ν (≈ 2 mHz) from the outer edges (larger θ) to ν of 5 mHz (3 minutes) and higher towards the cores of plages or umbrae of spots. These results for spots agree with those of earlier authors (McIntosh & Jefferies 2006; Zhao et al. 2016; Jess et al. 2016). Further, the results here show that plage structures too exhibit similar $\theta - \nu$ patterns for propagating waves and contrast them with those of the small-scale quiet-network fields.

3.2.2. Wave-energy Fluxes

As to the energy fluxes $F(\theta, \nu)$ and $F(B_{tot}, \nu)$, all magnetic structures show a similar ν dependence, which is dominantly determined by the background acoustic spectrum. Against inclination θ and strength B_{tot} , the influences of t_{ph} in F are clear: in the quiet-network,

F has a broad peak over θ extending from 20 to 70°, arising from the distinct wave-generation processes that we identified and discussed above in §3.2.1 as happening within the small-scale flux concentrations in addition to the magnetic inclination caused reduction in ν_{ac} ; otherwise, in the larger structures, plage and sunspot, F peaks at about $\theta = 60^\circ$, arising primarily from the filtering-in of ambient acoustic waves due to the reduced acoustic cut-off ν_{ac}^B . Theoretical studies of interaction between p-modes and magnetic fields identify this particular process, among several mode-conversion mechanisms (Cally *et al.* 2016), as one by which the incident acoustic waves continue along the magnetic fields as a slow acoustic mode, and has been termed as the ‘ramp effect’ (Cally 2007): this happens when the wave-vector is largely aligned or have small angles with magnetic field direction. Our results here, particularly the $\theta = 60^\circ$ peaked $F(\theta, \nu)$ shown in Figures 6 - 8, are in good agreement with the results from numerical simulations of mode-conversion processes in spot-like magnetic structures (Cally & Moradi 2013).

Except for the sunspot (lower panels of Figure 8), $F(B_{tot}, \nu)$ peak roughly around 100 G both in the quiet and plage regions. But, in the quiet-network, similar to the broad peak over θ , the peak in $F(B_{tot}, \nu)$ does extend over to larger B_{tot} for reasons discussed above. For the sunspot, the distinct smaller amplitude peak in F at ν centered around 6 mHz over the nearly vertical ($\nu < 20^\circ$) and strong field ($B_{tot} > 2500$ G) umbral region is clear in the lower panels of Figure 8; these correspond to the well-known 3-minute umbral oscillations.

3.3. Mean Wave-energy Fluxes

An important quantity that we can derive from our work here is the mean wave-energy flux over the region of observation, especially at low (2 - 5 mHz) frequencies where the magnetic fields play key roles (Jefferies *et al.* 2006), both in channelling such waves from the ambient medium and in generating them in-situ. As our foregoing analyses and results show with sufficient clarity, the multi-height observables provided by the HMI and AIA (1700 Å and 1600 Å) instruments, along with the photospheric vector magnetic fields, form an excellent set of data to estimate the wave-energy supply to the chromospheric layers. Energy flux estimates, in our method here, depend on the atmospheric height ranges Δz and Δz_v and the density scale-height H_ρ used for calculating group velocities v_g and velocity power P at chromospheric heights. As detailed in §2.3, although the method of calculations here is entirely different from that of Fossum & Carlsson (2005b), the 5.2 - 10 mHz quiet-Sun mean wave-energy flux that we derive, for a realistic set of values of $\Delta z = 190$ km, $\Delta z_v = 210$ km and $H_\rho = 110$ km corresponding to AIA 1700 Å height of 360 km, is 286.2 W m⁻² (refer to Figure 11), the same as estimated by Fossum & Carlsson (2005b) and Jefferies *et al.* (2006). This agreement, without any additional scaling as done by Jefferies *et al.* (2006) to calibrate their estimates, makes our estimates for the lower frequency (2 - 5.2 mHz) energy fluxes directly comparable with that of these authors. Again, as pointed out in §2.3, although the 5.2 - 10 mHz energy flux is likely an underestimate by a factor of $\approx e$ for $\nu > \nu_{ac}$, use of magnetically modified evolution of velocities in height $\exp[\Delta z_v/4H_\rho]$,

rather than $\exp[\Delta z_v/2H_\rho]$, is important when much of the propagation at $\nu < \nu_{ac}$ is within magnetic fields as observed here (*cf.* Figures 3 - 5). However, to the extent that there could be other physical causes than the magnetic fields, for example, non-adiabaticity, for wave propagation at $\nu < \nu_{ac}$, our estimates likely are lower limits.

The mean energy fluxes against frequency over the quiet, plage and spot areas estimated at the two heights, 360 and 430 km, are shown in Figure 11. The results for the quiet-network in Figure 11 is for the rectangular sub-region enclosed by the blue dotted-line boundary within the August 03, 2010 region shown in Figure 1. At height 360 km (AIA 1700 Å), using the above values for Δz , Δz_v and H_ρ that give a flux of 286.2 W m⁻² over 5.2 - 10 mHz, the 2 - 5.2 mHz quiet-Sun mean energy flux is 2251.5 W m⁻². And, at height 430 km (AIA 1600 Å), where we have $\Delta z = 260$ km, $\Delta z_v = 280$ km and the same $H_\rho = 110$ km, the mean energy fluxes over 5.2 - 10 mHz and 2 - 5.2 mHz are 243.6 W m⁻² and 2592.0 W m⁻², respectively. The above 2 - 5.2 mHz quiet-Sun mean energy fluxes in the range of 2.25 - 2.6 kW m⁻² is about twice that reported by Jefferies *et al.* (2006) for the same range of heights as probed here. Our estimated range for the low-frequency wave-energy supply facilitated by the quiet-Sun magnetic field is, thus, a much larger fraction of that required for balancing the average quiet-chromospheric radiative losses of 4.6 kW m⁻² according to the semi-empirical VAL3-C model of Vernazza *et al.* (1981).

As shown and discussed in §3.2.1, we have deduced that the operation of a mechanism different from that due to magnetic inclination assisted propagation of low-frequency (2 - 5.2 mHz) waves within the small-scale quiet network and which produces waves that evolve faster to steepen at the lower chromospheric heights is necessary. It is instructive to estimate the contribution by this new mechanism in comparison to that due to reduced cut-off frequency. In the quiet-Sun energy flux maps shown in the lower left panels of Figure 6, we take a ratio of flux summed over all locations where $\theta < \theta_{ac} = \cos^{-1}(\nu/\nu_{ac})$ to that over the whole region. The results are plotted in the right panel of Figure 9, for both the heights. At 3 mHz and at 360 km, up to about 32% of the energy flux over the whole region is contributed by waves, which are propagating within the small-scale magnetic fields where the inclination $\theta < \theta_{ac}$ and hence are not the ambient acoustic waves let through via the reduction in acoustic cut-off. Over the 2 - 5.2 mHz range, the net energy flux by such waves is about 25%. At 430 km, the energy flux of $\theta < \theta_{ac}$ waves is smaller at about 20% of that of the whole region.

The mean wave-energy fluxes over the plage and spot regions too have been estimated and are shown in Figure 11. The larger flux concentrations, due to larger areas of inclined fields, allow a larger flux of acoustic waves, and the numbers are marked within the panels of Figure 11. The interesting reduction in the fluxes of higher frequency (5.2 - 10 mHz) waves is due to the large-scale ‘shadows’ around these large structures, clearly seen in the right panels of Figures 4 and 5, and are associated with the magnetic canopy around them. The missing energy at chromospheric levels could perhaps be the reason for the enhanced power of photospheric high-frequency

waves called the ‘acoustic halos’ (see Rajaguru et al. 2013, and reference therein), which have been modeled as due to fast-wave refraction (Rijs et al. 2016).

4. SUMMARY AND DISCUSSION

In this paper, we have studied in detail the relationships between magnetic fields and (magneto-)acoustic wave-propagation in the lower solar atmosphere utilising the excellent quality data provided by the instruments HMI and AIA onboard SDO. We have estimated phase travel-times of acoustic waves in the atmosphere using cross-spectra of intensities between two heights, used them to derive group velocities of these waves, and combined them with wave-power derived from velocity data (HMI) to calculate energy fluxes. We have examined in detail the relations between the above derived quantities and the vector magnetic field – inclination and strength – in quiet, plage and sunspot regions. While establishing connections with and confirming several known results in the literature as discussed in the sub-sections of §3, we have also derived some new results, which we summarise below.

(1) Between the upper photospheric heights of 150 - 170 km (velocities and intensities observed by SDO/HMI) and lower chromospheric heights of 360 - 430 km (1700 Å and 1600 Å intensities observed by SDO/AIA), we have identified and shown that the relatively less-inclined, nearly vertical magnetic field elements in the quiet-Sun channel a significant amount of acoustic waves of frequencies, in the range of 2 - 4 mHz, that are smaller than the theoretical minimum for the reduction in acoustic cut-off due to magnetic inclination (§3.2.1, Figures 6 and 7)(Bel & Leroy 1977).

(2) Between the heights of 360 and 430 km, the phase travel times of the above low frequency waves within the isolated and nearly vertical magnetic elements do not show an increase expected over height, rather a decrease for the lowest frequencies (2 - 2.5 mHz), (*c.f.*, Figure 9, left panel), indicating wave-steepening or dissipation.

(3) Propagating waves observed within the larger magnetic structures, plages and a sunspot, confirm to the reduction in cut-off due to magnetic inclination, *i.e.*, obey the relation $\nu_{ac}^B = \nu_{ac} \cos\theta$ for the minimum ν of propagation (Bel & Leroy 1977; McIntosh & Jefferies 2006), and do not exhibit the characteristics described in (1) and (2) above. Instead, phase travel times of waves propagating along the inclined field do increase through the height ranges probed indicating propagation beyond 430 km.

(4) The energy flux of acoustic waves within magnetic structures, small and large, peak around magnetic inclination $\theta = 60^\circ$ (bottom panels, Figures 6 - 8), except that the small-scale quiet-Sun magnetic fields exhibit a broader peak extending down to $\theta \approx 20^\circ$ (bottom left panel, Figure 6). This result for the larger structures provides an observational verification of the numerical simulations of mode-conversion process, especially the ramp effect (Cally & Moradi 2013).

(5) The mean energy flux over the quiet-Sun (or quiet magnetic network), over the 2 - 5 mHz frequency region, between the upper photosphere and heights corresponding to AIA 1700 Å and 1600 Å intensities is in the range of 2.25 to 2.6 kW m⁻² (§3.3, Figure 11), which is about twice the previous estimates (Jefferies et al. 2006). Out of this total quiet-Sun acoustic flux, about 25 to 30%

is due to the newly identified wave-propagation process summarised in results (1) and (2) above (right panel, Figure 9).

Since the waves of frequencies 2 - 4 mHz found in result (1) are lower than the theoretical minimum given by $\nu_{ac}^B = \nu_{ac} \cos\theta$ they certainly are not the ambient acoustic waves propagating because of magnetic-inclination-assisted cut-off frequency reduction. We, in §3.1, ruled out artifacts or contamination due to height-dependent RD as the cause of result (1). And, in §3.2.1, we discussed the connections between our result (1) and the observations and models based on RD by Centeno et al. (2006) and Khomenko et al. (2008) on the one hand and those of Giovanelli et al. (1978) and Roberts (1983) on the other. Both the above earlier observational results show increasing t_{ph} over heights that extend well above the range covered here and hence are in contrast with our result (2), *viz.* the low-frequency (2 - 4 mHz) waves within the small-scale near-vertical magnetic fields evolve over height faster (*i.e.*, shorter t_{ph}) than the ambient acoustic waves do along inclined magnetic fields – this particular property indeed is seen in some wave simulation studies and we come back to it in the next paragraph. We note that the above propagating waves within the near-vertical fields are accompanied by the slightly larger, but still well below the quiet-Sun acoustic cut-off, frequency waves in the inclined boundaries of the same small-scale magnetic structures with their t_{ph} (Figure 6, top right panel for quiet-Sun) increasing over height. It should be pointed out that the above earlier authors did not have magnetic inclination information in their observations and hence it was not clear that the increasing t_{ph} signals at the low frequencies that they measure at higher in the chromosphere were still associated with that of RD origin in photospheric vertical magnetic field; at heights above 500 km, vertical flux tubes must have expanded to fill the chromospheric volume and hence waves let out due to inclined magnetic field might spatially overlap with those propagating due to RD and in addition, mode conversion between fast modes to slow waves or between kink modes to slow modes will confuse the identification of the origin of propagating waves. Hence, the scenario presented by our results (1) and (2) together appear distinct from that of above authors’ observational results. However, as discussed in detail in §3.2.1, we do find that the case of the tube mode (or sausage mode) subject to strong photospheric RD as theorised by Roberts (1983) provides an interesting explanation for result (1), although a detailed study of non-linear development and shock-formation of the tube mode subject to RD is necessary to explain results (1) and (2) together. Further, for flux elements of small horizontal size, a careful treatment of horizontal radiative exchange is important while treating the RD due to vertical radiative losses, because such multi-dimensional radiative transfer can vastly modify the wave motions (Kneer & Trujillo-Bueno 1987), *e.g.* making the waves overstable (countering the RD) (Moore & Spiegel 1966; Massaglia et al. 1989; Rajaguru & Hasan 2000).

An alternative possibility is the in-situ wave generation process, accompanied by changes in the atmospheric stratification within the magnetic elements so as to allow propagation at frequencies well below the acoustic cut-off. Moreover, since result (3) shows that such low-frequency propagation is not seen within the cores (or less inclined

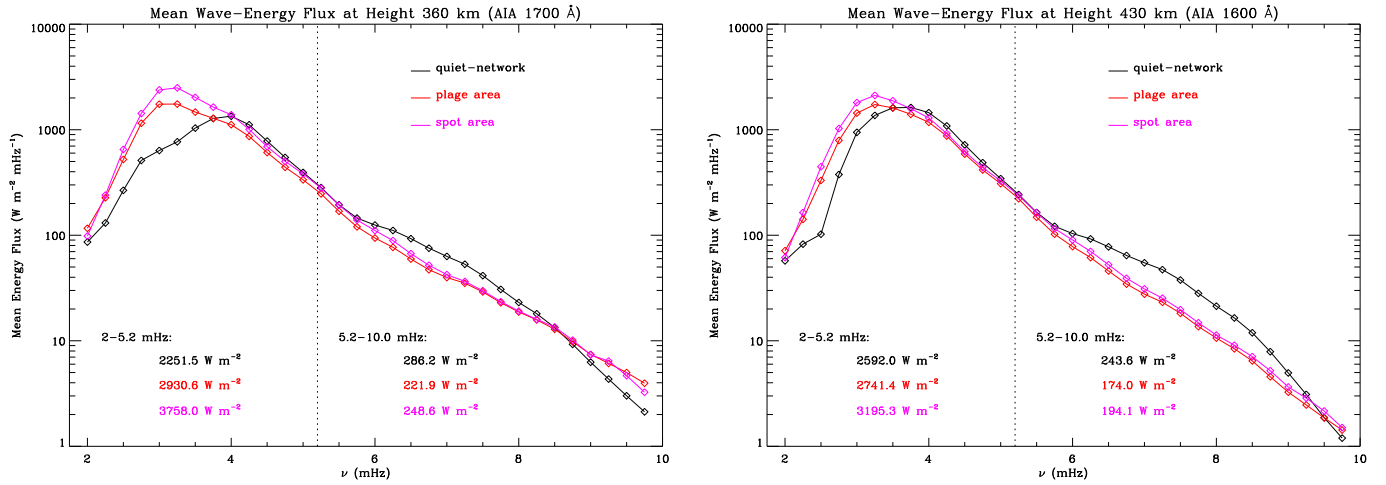


Figure 11. Mean wave-energy fluxes against frequency at heights 360 km (AIA 1700 Å, left panel) and 430 km (AIA 1600 Å, right panel). The three curves, black, red and pink correspond to mean fluxes over quiet-network, plage and spot areas, respectively. In each panel, we have marked the frequency integrated fluxes over 2 - 5.2 mHz and 5.2 - 10 mHz ranges. The vertical dotted line marks the quiet-Sun acoustic cut-off frequency of 5.2 mHz. See text for full discussion.

central regions) of larger structures, plages and sunspot, the above in-situ process must be related to the flux elements being small (horizontally). The long-period network oscillations within the quiet magnetic-network as originally observed by Lites *et al.* (1993) have peak frequencies around 2.5 mHz (≈ 7 minutes) coinciding with our finding of dominant propagating waves in this same frequency range (Figure 6, *top left panel*). There have been a lot of work, in the literature, that addresses generation of waves within flux tubes or sheaths due to the buffeting action of external convection or waves (Choudhuri *et al.* 1993; Musielak *et al.* 1995; Hasan & Kalkofen 1999; Bogdan *et al.* 2003; Hasan *et al.* 2003; Hasan & van Ballegoijen 2008; Vigeesh *et al.* 2009) or in-situ generation within them by magneto-convective processes (Kato *et al.* 2011, 2016). The dominant periods of longitudinal (acoustic) waves generated within the flux tubes or sheaths in the above two distinct mechanisms are quite different: the former one utilising an external driving, either by transverse motions imparted by granules or through coupling with the ambient p modes, predict longitudinal waves of frequencies larger or at the tube cut-off frequency (Spruit 1981; Hasan & Kalkofen 1999), which is nearly the same as quiet-Sun acoustic cut-off of ≈ 5.2 mHz (3 minutes). However, the latter magneto-convective process within flux tubes or sheaths drive upward propagating longitudinal waves over a broad frequency range, 1 - 10 mHz, with peak power around 4 mHz (Kato *et al.* 2016), providing possible explanations for our observational results in Figures 6 and 7 for the quiet-network. We do note that Kato *et al.* (2016) indeed invoke possible contributions of magnetic inclination for the existence of low-frequency (<5.2 mHz) oscillations while cautioning that the simple estimates of acoustic cut-off frequency (Spruit 1981) do not hold good in the non-linear wave evolution typical in the atmospheric layers. Further, although the transverse motions of flux tubes or sheaths excite longitudinal tube modes that propagate at or above the cut-off frequency (5 mHz), Hasan & van Ballegoijen (2008) do point out

the possibility of the kink mode of much lower cut-off frequency (around 3.3 mHz) mode-converting to cause longitudinal waves at chromospheric heights. This again cannot explain our observations as we have longitudinal waves propagating from photospheric heights at frequencies well below 3.3 mHz. We however note that the simulations of Hasan & van Ballegoijen (2008) show an important difference between longitudinal waves excited within flux tubes by transverse motions and those, from the ambient acoustic waves, propagating along inclined field lines: the former evolve quickly to become shocks at chromospheric heights whereas the latter propagate through to higher layers. Our result (2) confirms this behaviour, although the observed longitudinal waves are well below the cut-off frequency.

In summary, the RD mechanism acting on the tube or sausage mode (Roberts 1983) or the one due to magneto-convective processes (Kato *et al.* 2011, 2016) discussed in the above two paragraphs, respectively, are relevant for the observations here. We, however, caution that more detailed examination, with multi-height velocity and intensity data, of our observational findings as well as the above theoretical and numerical models is necessary to pinpoint the exact mechanisms behind the low-frequency (lower than the theoretical minimum allowed by magnetic inclination) longitudinal propagating waves in the small-scale magnetic fields (Figure 6). As regards the role of small-scale magnetic fields, which Jefferies *et al.* (2006) called as magneto-acoustic portals, our result (5) shows that about half of 4.6 kW m⁻² (Vernazza *et al.* 1981) required to balance the average quiet-chromospheric radiative losses is carried by the energetic low frequency (2 - 5.2 mHz) acoustic waves harbored by them. Our results thus further corroborate the role of small-scale magnetic fields in chromospheric heating and in explaining the basal flux of emissions (Schrijver *et al.* 1989; Fossum & Carlsson 2005b).

Extensions of the study reported here would benefit a lot from a much finer height coverage of the photosphere - chromosphere region. Currently being built Solar Ultraviolet Imaging Telescope (SUIT Ghosh *et al.* 2016;

Tripathi et al. 2017) for the upcoming Aditya-L1 mission of the Indian Space Research Organisation (ISRO) will have such capabilities: imaging the Sun within the wavelength band of 2000–4000 Å covered by 11 different filters providing near-simultaneous observations.

C.R.S. and D.T. acknowledge support from the Max-Planck India Partner Group of MPS on “Coupling and Dynamics of the Solar Atmosphere” at IUCAA. The partner group is funded by MPG and DST(IGSTC), Gov. of India. Data-intensive numerical computations required in this work were carried out using the High Performance Computing facility of the Indian Institute of Astrophysics, Bangalore. This work has utilised extensively the HMI/SDO and AIA/SDO data pipeline at the Joint Science Operations Center (JSOC), Stanford University. We also thank an anonymous referee of this paper for prompting us to address the effects of radiative damping.

REFERENCES

- Alfvén, H. 1947, *MNRAS*, 107, 211
- Bel, N., & Leroy, B. 1977, *A&A*, 55, 239
- Biermann, L. 1946, *Naturwissenschaften*, 33, 118
- Bogdan, T. J., Carlsson, M., Hansteen, V. H., et al. 2003, *ApJ*, 599, 626
- Borrero, J.H., Tomczyk, S., Kubo, M., Socas-Navarro, H., Schou, J., Couvidat, S., Bogart, R.: 2011, *Sol. Phys.* **273**, 267
- Cally, P. S., & Bogdan, T. J. 1997, *ApJL*, 486, L67
- Cally, P. S. 2007, *Astronomische Nachrichten*, 328, 286
- Cally, P. S., Moradi, H., & Rajaguru, S. P. 2016, *Washington DC American Geophysical Union Geophysical Monograph Series*, 216, 489
- Cally, P. S., & Moradi, H. 2013, *MNRAS*, 435, 2589
- Canfield, R. C., & Musman, S. 1973, *ApJL*, 184, L131
- Centeno, R., Collados, M., & Trujillo Bueno, J. 2006, *Solar Polarization* 4, 358, 465
- Centeno, R., Collados, M., & Trujillo Bueno, J. 2009, *ApJ*, 692, 1211
- Chandra, R., Gupta, G. R., Mulay, S., & Tripathi, D. 2015, *MNRAS*, 446, 3741
- Choudhuri, A. R., Auffret, H., & Priest, E. R. 1993, *Sol. Phys.*, 143, 49
- Jørgen Christensen-Dalsgaard, *Lecture Notes on Stellar Oscillations* 2003 (Fifth Edition), <http://users-phys.au.dk/jcd/oscilnotes/>
- Couvidat, S., Rajaguru, S. P., Wachter, R., et al. 2012, *Sol. Phys.*, 278, 217
- De Moortel, I., & Rosner, R. 2007, *Sol. Phys.*, 246, 53
- De Pontieu, B., Erdélyi, R., & James, S. P. 2004, *Nature*, 430, 536
- De Pontieu, B., Erdélyi, R., & De Moortel, I. 2005, *ApJL*, 624, L61
- de Wijn, A. G., Rutten, R. J., & Tarbell, T. D. 2005, *A&A*, 430, 1119
- Deubner, F.-L., Fleck, B., Marmolino, C., & Severino, G. 1990, *A&A*, 236, 509
- Duvall, T. L., Jr., Jefferies, S. M., Harvey, J. W., Osaki, Y., & Pomerantz, M. A. 1993, *ApJ*, 410, 829
- Finsterle, W., Jefferies, S. M., Cacciani, A., et al. 2004, *Sol. Phys.*, 220, 317
- Fleck, B., Couvidat, S., & Straus, T. 2011, *Sol. Phys.*, 271, 27
- Fontenla, J. M., Avrett, E. H., & Loeser, R. 1993, *ApJ*, 406, 319
- Fossum, A., & Carlsson, M. 2005a, *ApJ*, 625, 556
- Fossum, A., & Carlsson, M. 2005b, *Nature*, 435, 919
- Ghosh, A., Chatterjee, S., Khan, A. R., et al. 2016, *Proc. SPIE*, 9905, 990503
- Giles, P. M. 2000, Ph.D. Thesis, 891
- Giovanelli, R. G., Livingston, W. C., & Harvey, J. W. 1978, *Sol. Phys.*, 59, 49
- Bello González, N., Flores Soriano, M., Kneer, F., & Okunev, O. 2009, *A&A*, 508, 941
- Bello González, N., Yelles Chaouche, L., Okunev, O., & Kneer, F. 2009, *A&A*, 494, 1091
- Bello González, N., Flores Soriano, M., Kneer, F., Okunev, O., & Shchukina, N. 2010, *A&A*, 522, A31
- Handy, B. N., Acton, L. W., Kankelborg, C. C., et al. 1999, *Sol. Phys.*, 187, 229
- Hasan, S. S., & Kalkofen, W. 1999, *ApJ*, 519, 899
- Hasan, S. S., Kalkofen, W., van Ballegooijen, A. A., & Ulmschneider, P. 2003, *ApJ*, 585, 1138
- Hasan, S. S., & van Ballegooijen, A. A. 2008, *ApJ*, 680, 1542
- Hill, F., Deubner, F.-L., & Isaak, G. 1991, *Solar Interior and Atmosphere*, 329
- Hoeksema, J. T., Liu, Y., Hayashi, K., et al. 2014, *Sol. Phys.*, 289, 3483
- Jefferies, S. M., McIntosh, S. W., Armstrong, J. D., et al. 2006, *ApJL*, 648, L151
- Jess, D. B., Reznikova, V. E., Ryans, R. S. I., et al. 2016, *Nature Physics*, 12, 179
- Kalkofen, W. 2007, *ApJ*, 671, 2154
- Kato, Y., Steiner, O., Steffen, M., & Suematsu, Y. 2011, *ApJL*, 730, L24
- Kato, Y., Steiner, O., Hansteen, V., et al. 2016, *ApJ*, 827, 7
- Kayshap, P., Srivastava, A. K., Murawski, K., & Tripathi, D. 2013, *ApJL*, 770, L3
- Khomenko, E., Centeno, R., Collados, M., & Trujillo Bueno, J. 2008, *ApJL*, 676, L85
- Khomenko, E., & Calvo Santamaria, I. 2013, *Journal of Physics Conference Series*, 440, 012048
- Kitagawa, N., Yokoyama, T., Imada, S., & Hara, H. 2010, *ApJ*, 721, 744
- Klimchuk, J. A. 2006, *Sol. Phys.*, 234, 41
- Kneer, F., & Trujillo-Bueno, J. 1987, *A&A*, 183, 91
- Krijger, J. M., Rutten, R. J., Lites, B. W., et al. 2001, *A&A*, 379, 1052
- Leka, K.D., Barnes, G., Crouch, A.D., Metcalf, Thomas R., Gary, G. Allen, Jing, Ju, Liu, Y.: 2009, *Sol. Phys.*, 260, 83.
- Lemen, J. R., Title, A. M., Akin, D. J., et al. 2012, *Sol. Phys.*, 275, 17
- Lighthill, M. J. 1952, *Proceedings of the Royal Society of London Series A*, 211, 564
- Linsky, J. L. 2017, *ARA&A*, 55, 159
- Lites, B. W., Rutten, R. J., & Kalkofen, W. 1993, *ApJ*, 414, 345
- Massaglia, S., Rossi, P., & Bodo, G. 1989, *A&A*, 209, 399
- McIntosh, S. W., & Jefferies, S. M. 2006, *ApJL*, 647, L77
- Metcalf, T.R. 1994, *Sol. Phys.*, 155, 235.
- Metcalf, T.R., Leka, K.D., Barnes, G., Lites, B.W., Georgoulis, M.K., Pevtsov, A.A., Balasubramaniam, K.S., et al. 2006, *Sol. Phys.*, 237, 267.
- Mihalas, B. W., & Toomre, J. 1982, *ApJ*, 263, 386
- Moore, D. W., & Spiegel, E. A. 1966, *ApJ*, 143, 871
- Musielak, Z. E., Rosner, R., Gail, H. P., & Ulmschneider, P. 1995, *ApJ*, 448, 865
- Nagashima, K., Löptien, B., Gizon, L., et al. 2014, *Sol. Phys.*, 289, 3457
- Narain, U., & Ulmschneider, P. 1996, *Space Sci. Rev.*, 75, 453
- Newington, M. E., & Cally, P. S. 2011, *MNRAS*, 417, 1162
- Nigam, R., & Kosovichev, A. G. 1999, *ApJL*, 510, L149
- Norton, A. A., Graham, J. P., Ulrich, R. K., et al. 2006, *Sol. Phys.*, 239, 69
- Noyes, R. W., Hartmann, L. W., Baliunas, S. L., Duncan, D. K., & Vaughan, A. H. 1984, *ApJ*, 279, 763
- Nutto, C., Steiner, O., Schaffenberger, W., & Roth, M. 2012, *A&A*, 538, A79
- Osterbrock, D. E. 1961, *ApJ*, 134, 347
- Parker, E. N. 1991, *ApJ*, 376, 355
- Rajaguru, S. P., & Hasan, S. S. 2000, *ApJ*, 544, 522
- Rajaguru, S. P., Hughes, S. J., & Thompson, M. J. 2004, *Sol. Phys.*, 220, 381
- Rajaguru, S. P., Sankarasubramanian, K., Wachter, R., & Scherrer, P. H. 2007, *ApJL*, 654, L175
- Rajaguru, S. P., Wachter, R., Sankarasubramanian, K., & Couvidat, S. 2010, *ApJL*, 721, L86
- Rajaguru, S. P., Couvidat, S., Sun, X., Hayashi, K., & Schunker, H. 2013, *Sol. Phys.*, 287, 107
- Rijs, C., Rajaguru, S. P., Przybylski, D., et al. 2016, *ApJ*, 817, 45
- Roberts, B. 1983, *Sol. Phys.*, 87, 77
- Roberts, B. 2006, *Philosophical Transactions of the Royal Society of London Series A*, 364, 447
- Rosenthal, C. S., Bogdan, T. J., Carlsson, M., et al. 2002, *ApJ*, 564, 508
- Schmieder, B. 1978, *Sol. Phys.*, 57, 245
- Scherrer, P. H., Bogart, R. S., Bush, R. I., et al. 1995, *Sol. Phys.*, 162, 129
- Scherrer, P. H., Schou, J., Bush, R. I., et al. 2012, *Sol. Phys.*, 275, 207
- Schou, J., Scherrer, P. H., Bush, R. I., et al. 2012, *Sol. Phys.*, 275, 229
- Schrijver, C. J., Dobson, A. K., & Radick, R. R. 1989, *ApJ*, 341, 1035
- Schunker, H., & Cally, P. S. 2006, *MNRAS*, 372, 551
- Schunker, H., & Braun, D. C. 2011, *Sol. Phys.*, 268, 349
- Schwarzschild, M. 1948, *ApJ*, 107, 1
- Severino, G., Magri, M., Oliviero, M., Straus, T., & Jefferies, S. M. 2001, *ApJ*, 561, 444

- Severino, G., Straus, T., Oliviero, M., Steffen, M., & Fleck, B. 2013, *Sol. Phys.*, 284, 297
- Skartlien, R., & Rast, M. P. 2000, *ApJ*, 535, 464
- Socas-Navarro, H. 2005, *ApJL*, 633, L57
- Souffrin, P. 1972, *A&A*, 17, 458
- Spiegel, E. A. 1957, *ApJ*, 126, 202
- Spruit, H. C. 1981, *A&A*, 98, 155
- Spruit, H. C. 1982, *Sol. Phys.*, 75, 3
- Staiger, J., Mattig, W., Schmieder, B., & Deubner, F.-L. 1984, *Mem. Soc. Astron. Italiana*, 55, 147
- Staiger, J. 1985, Ph.D. Thesis, University of Freiburg i. Br.
- Stein, R. F. 1967, *Sol. Phys.*, 2, 385
- Stein, R. F. 1968, *ApJ*, 154, 297
- Straus, T., Fleck, B., Jefferies, S. M., et al. 2008, *ApJL*, 681, L125
- Tripathi, D., Reeves, K. K., Gibson, S. E., Srivastava, A., & Joshi, N. C. 2013, *ApJ*, 778, 142
- Tripathi, D., Ramaprakash, A. N., Khan, A. R., et al. 2017, *Current Science*, 113, 616
- Ulmschneider, P. 1990, *Cool Stars, Stellar Systems, and the Sun*, 9, 3
- Ulmschneider, P., & Musielak, Z. 2003, *Current Theoretical Models and Future High Resolution Solar Observations: Preparing for ATST*, 286, 363
- Vecchio, A., Cauzzi, G., Reardon, K. P., Janssen, K., & Rimmele, T. 2007, *A&A*, 461, L1
- Vernazza, J. E., Avrett, E. H., & Loeser, R. 1981, *ApJS*, 45, 635
- Vigeesh, G., Hasan, S. S., & Steiner, O. 2009, *A&A*, 508, 951
- Webb, A. R., & Roberts, B. 1980, *Sol. Phys.*, 68, 87
- Wiśniewska, A., Musielak, Z. E., Staiger, J., & Roth, M. 2016, *ApJL*, 819, L23
- Zhao, J., Felipe, T., Chen, R., & Khomenko, E. 2016, *ApJL*, 830, L17